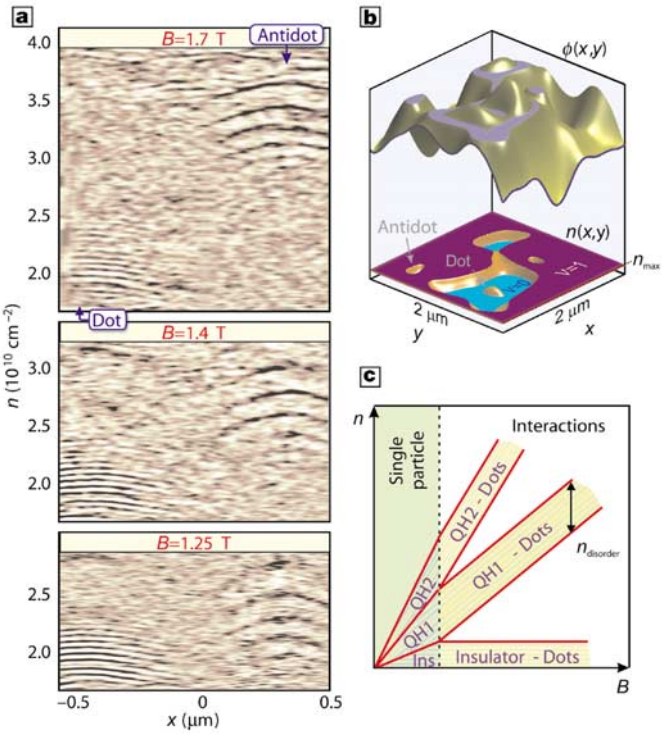

Figure 4 Localized states in the presence of strong disorder. **a**, Density–position scans at $B = 1.7$ T, 1.4 T, 1.25 T tracking a $\nu = 1$ antidot and $\nu = 0$ dot down to the highly disordered regime at low B ($\Delta n_{\text{disorder}} \gg n_{\text{max}}$). The highest density in all scans corresponds to $\nu = 1$. At the lowest B, both dot and antidot coexist—hole-like $\nu = 1$ states neighbour electron-like $\nu = 0$ states less than 1 μm away. **b**, Self-consistent Thomas–Fermi calculation in the limit of strong disorder. Here, the disorder creates large density fluctuations, which force the Landau level to be either completely empty or completely full and therefore incompressible. Compressible pockets in the $\nu = 0$ and $\nu = 1$ plateaus result in $\nu = 0$ dots and $\nu = 1$ antidots, as marked in the figure. On the boundary between the $\nu = 0$ and $\nu = 1$ regions a narrow compressible strip exists, following a constant energy contour of the bare disorder potential. **c**, A generalized phase diagram for QH-localization as deduced from our measurements. At low B, localized states are dominated by disorder and follow the single-particle phenomenology. Here the familiar QH phase transitions at half-filling of Landau levels are observed. At higher fields, interactions prevail and localized states form within dots or antidots. In this regime, new percolation phase boundaries emerge (red lines) and limit the QH phenomena to strips of width $\Delta n_{\text{disorder}}$ centred around their corresponding filling factors.

We summarize our results in a generalized phase diagram of localization in the QH regime (Fig. 4c). The disorder in any given sample is characterized by $\Delta n_{\text{disorder}}$ irrespective of the density. Depending on the interaction strength relative to the disorder, localized states acquire a different nature. When disorder is strong or when B is small ($\Delta n_{\text{disorder}} \gg n_{\text{max}}$), localized states are narrow compressible strips, which obey the single-particle phenomenology. Consequently, the familiar QH phase transitions exist at half-filling of the Landau levels. This explains why single-particle scaling of QH transitions is observed only in highly-disordered samples[3–9]. At higher magnetic fields, localization is dominated by interactions and localized states form within dots or antidots. In this regime, new percolation phase boundaries emerge (red lines in Fig. 4c), limiting the QH phenomena to strips of width $\Delta n_{\text{disorder}}$ centred around the QH filling factors. □

Received 26 August; accepted 21 November 2003; doi:10.1038/nature02230.

1. Prange, R. E. & Girvin, S. M. *The Quantum Hall Effect* (Springer, New York, 1990).
2. Huckestein, B. Scaling theory of the integer quantum Hall-effect. *Rev. Mod. Phys.* **67,** 357–396 (1995).
3. Wei, H., Tsui, D., Paalanen, M. & Pruisken, A. Experiments on delocalization and universality in the integral quantum Hall effect. *Phys. Rev. Lett.* **61,** 1294–1296 (1988).
4. Wei, H. P., Lin, S. Y., Tsui, D. C. & Pruisken, A. M. M. Effect of long-range potential fluctuations on scaling in the integer quantum Hall-effect. *Phys. Rev. B* **45,** 3926–3928 (1992).
5. Engel, L., Wei, H. P., Tsui, D. C. & Shayegan, M. Critical exponent in the fractional quantum Hall-effect. *Surf. Sci.* **229,** 13–15 (1990).
6. Koch, S., Haug, R., von-Klitzing, K. & Ploog, K. Size-dependent analysis of the metal-insulator transition in the integral quantum Hall effect. *Phys. Rev. Lett.* **67,** 883–886 (1991).
7. Engel, L. W., Shahar, D., Kurdak, C. & Tsui, D. C. Microwave frequency-dependence of integer quantum Hall-effect—evidence for finite-frequency scaling. *Phys. Rev. Lett.* **71,** 2638–2641 (1993).
8. Hohls, F., Zeitler, U. & Haug, R. Hopping conductivity in the quantum Hall effect: Revival of universal scaling. *Phys. Rev. Lett.* **88,** 1–4 (2002).
9. Hohls, F. *et al.* Dynamical scaling of the quantum Hall plateau transition. *Phys. Rev. Lett.* **89,** 1–4 (2002).
10. Shahar, D. *et al.* A new transport regime in the quantum Hall effect. *Solid State Commun.* **107,** 19–23 (1998).
11. Balaban, N., Meirav, U. & Bar-Joseph, I. Absence of scaling in the integer quantum Hall effect. *Phys. Rev. Lett.* **81,** 4967–4970 (1998).
12. Cobden, D. H., Barnes, C. H. W. & Ford, C. J. B. Fluctuations and evidence for charging in the quantum Hall effect. *Phys. Rev. Lett.* **82,** 4695–4698 (1999).
13. Chklovskii, D. B. & Lee, P. A. Transport properties between quantum Hall plateaus. *Phys. Rev. B* **48,** 18060–18078 (1993).
14. Cooper, N. R. & Chalker, J. T. Coulomb interactions and the integer quantum Hall-effect—screening and transport. *Phys. Rev. B* **48,** 4530–4544 (1993).
15. Ruzin, I., Cooper, N. & Halperin, B. Nonuniversal behavior of finite quantum Hall systems as a result of weak macroscopic inhomogeneities. *Phys. Rev. B* **53,** 1558–1572 (1996).
16. Ilani, S., Yacoby, A., Mahalu, D. & Shtrikman, H. Unexpected behavior of the local compressibility near the B = 0 metal-insulator transition. *Phys. Rev. Lett.* **84,** 3133–3136 (2000).
17. Yoo, M. J. *et al.* Scanning single-electron transistor microscopy: Imaging individual charges. *Science* **276,** 579–582 (1997).
18. Yacoby, A., Hess, H. F., Fulton, T. A., Pfeiffer, L. N. & West, K. W. Electrical imaging of the quantum Hall state. *Solid State Commun.* **111,** 1–13 (1999).
19. Zhitenev, N. B. *et al.* Imaging of localized electronic states in the quantum Hall regime. *Nature* **404,** 473–476 (2000).
20. Ilani, S., Yacoby, A., Mahalu, D. & Shtrikman, H. Microscopic structure of the metal-insulator transition in two dimensions. *Science* **292,** 1354–1357 (2001).
21. Efros, A. L. & Ioffe, A. F. Nonlinear screening and the background density of 2DEG states in magnetic field. *Solid State Commun.* **67,** 1019–1022 (1988).
22. Efros, A. L., Pikus, F. G. & Burnett, V. G. Density of states of a two-dimensional electron gas in a long-range random potential. *Phys. Rev. B* **47,** 2233–2243 (1993).
23. Shashkin, A. *et al.* Percolation metal-insulator transitions in the two-dimensional electron system of AlGaAs/GaAs heterostructures. *Phys. Rev. Lett.* **73,** 3141–3144 (1994).
24. Kukushkin, I., Fal'ko, V., Haug, R., von Klitzing, K. & Eberl, K. Magneto-optical evidence of the percolation nature of the metal-insulator transition in the two-dimensional electron system. *Phys. Rev. B* **53,** R13260–R13263 (1996).

Acknowledgements We benefited from discussions with A. M. Fink'elstein, Y. Gefen, Y. Meir, A. Stern and N. B. Zhitenev. This work was supported by the Israeli Science Foundation and the German MINERVA foundation.

Competing interests statement The authors declare that they have no competing financial interests.

Correspondence and requests for materials should be addressed to S.I. (shahal.ilani@cornell.edu).

The role of increasing temperature variability in European summer heatwaves

Christoph Schär[1], Pier Luigi Vidale[1], Daniel Lüthi[1], Christoph Frei[1], Christian Häberli[2], Mark A. Liniger[2] & Christof Appenzeller[2]

[1]*Atmospheric and Climate Science, ETH Zürich, Winterthurerstrasse 190, 8057 Zürich, Switzerland*
[2]*MeteoSwiss, Krähbühlstrasse 58, 8044 Zürich, Switzerland*

Instrumental observations[1,2] and reconstructions[3,4] of global and hemispheric temperature evolution reveal a pronounced warming during the past ~150 years. One expression of this warming is the observed increase in the occurrence of heatwaves[5,6]. Conceptually this increase is understood as a shift of the statistical distribution towards warmer temperatures, while changes in the width of the distribution are often considered small[7]. Here we

show that this framework fails to explain the record-breaking central European summer temperatures in 2003, although it is consistent with observations from previous years. We find that an event like that of summer 2003 is statistically extremely unlikely, even when the observed warming is taken into account. We propose that a regime with an increased variability of temperatures (in addition to increases in mean temperature) may be able to account for summer 2003. To test this proposal, we simulate possible future European climate with a regional climate model in a scenario with increased atmospheric greenhouse-gas concentrations, and find that temperature variability increases by up to 100%, with maximum changes in central and eastern Europe.

A record-breaking heatwave affected the European continent in summer 2003. In a large area, mean summer (June, July and August, referred to as JJA below) temperatures have exceeded the 1961–90 mean by ~3 °C, corresponding to an excess of up to 5 standard deviations (Fig. 1a). Even away from the centre of action, many long-standing temperature records have tumbled.

For further analysis, we consider long-term temperature series from Switzerland, located close to the centre of the anomaly. Twelve carefully homogenized series[8,9] are available with daily resolution since 1864. To minimize contamination by local meteorological and instrumental conditions, we amalgamate four independent and particularly reliable stations (Basel-Binningen, Geneva, Bern-Liebefeld, and Zürich) into one single series with monthly temporal resolution. This series is representative for the northwestern foothills of the Alps. Figure 1b–e displays the statistical distribution of monthly and seasonal temperatures. The year 2003 is far off the distribution in three of the four panels. For instance, the previous record holder for JJA was 1947 with a temperature anomaly of $T' = 2.7$ °C (with respect to the 1864–2000 mean). The corresponding value for 2003 is as high as $T' = 5.1$ °C and this amounts to an offset of 5.4 standard deviations from the mean (the corresponding values of individual months are listed in Fig. 1). Such extreme values (which indeed have the characteristics of outliers) pose serious challenges to any analysis, as the statistical distribution so far away from the mean is not described by the data.

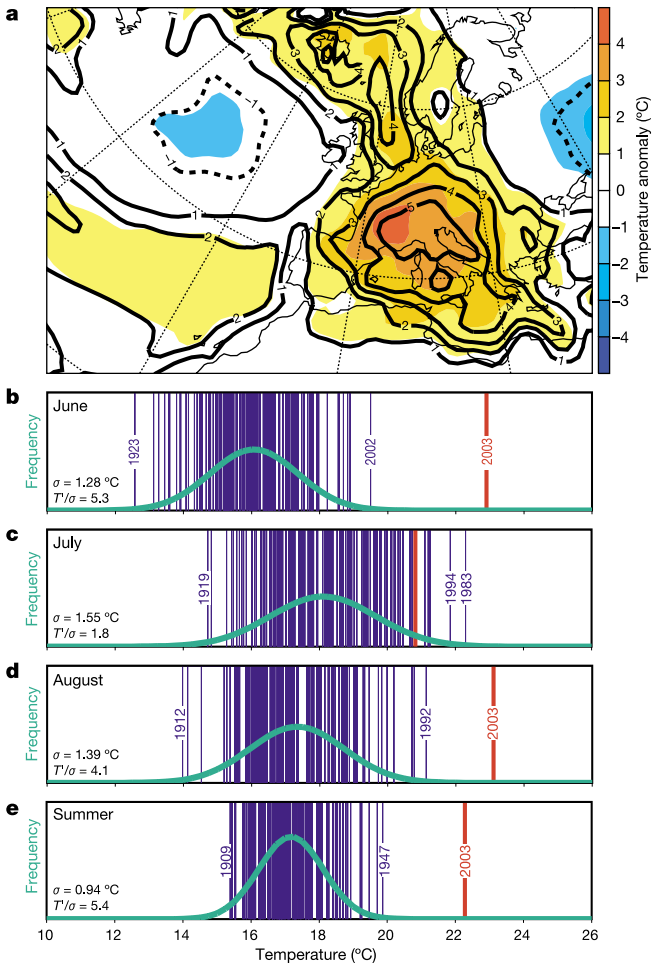

Figure 1 Characteristics of the summer 2003 heatwave. **a**, JJA temperature anomaly with respect to the 1961–90 mean. Colour shading shows temperature anomaly (°C), bold contours display anomalies normalized by the 30-yr standard deviation. **b**–**e**, Distribution of Swiss monthly and seasonal summer temperatures for 1864–2003. The fitted gaussian distribution is indicated in green. The values in the lower left corner of each panel list the standard deviation (σ) and the 2003 anomaly normalized by the 1864–2000 standard deviation (T'/σ). See Methods section for further details.

In a first step, we thus restrict attention to the time period 1864–2000 and compile compound statistics for all monthly temperature anomalies (January–December). The purpose of this is to identify changes near the tails of the statistical distribution that result from the warming trend in the series. To this end, we consider two 60-yr periods, one covering the beginning of the series (1864–1923), and one the end (1941–2000). Figure 2a, b shows the resulting statistical distributions, both in terms of cumulative probability and probability density functions. The two distributions show similar characteristics in general, but the 1941–2000 distribution is shifted by the mean warming ($\Delta T = 0.8$ °C) between the two periods. This shift also implies a change in the frequency of extremes. For instance (Fig. 2c), the frequency of a month with an anomaly of $T' = 3$ °C has increased by ~100%. Hence, a month in the 1941–2000 period with an excess temperature of $T' = 3$ °C can be tied with a probability of 50% to the warming between the two periods, in a probabilistic sense as recently proposed[10]. This illustrates how comparatively small shifts in climate mean may imply pronounced changes at the tails of the statistical distribution and in the frequency of extremes.

The dashed and full curves in Fig. 2 relate to the empirical and the fitted gaussian distributions, respectively, and their close agreement shows that the gaussian distribution is an excellent approximation to the data. The small reduction in variability (Fig. 2b) is not statistically significant, and is entirely due to changes in the month of December (where the variability was substantially reduced owing to the absence of cold northeasterly weather types).

A conclusive analysis such as that in Fig. 2 is not feasible for summer 2003, as there is only one data point so far off the mean. To quantitatively assess the situation, we have estimated its return period. The return period τ is an estimate of the frequency of a particular event (or its exceedance) based on a stochastic concept. Here we employ a gaussian distribution fitted to JJA temperatures to estimate τ with respect to a selected reference period (see Methods section for details). With respect to the reference period 1864–2000, a return period of several million years is obtained, but such an excessive estimate based on a short series is dubious. To account for the warming in the last decades, we use a more recent reference period 1990–2002 (with $\Delta T = 1.25$ °C warmer mean temperature, but assuming an unchanged standard deviation). With respect to this climatology, the resulting return period for summer 2003 still amounts to $\tau = 46{,}000$ yr. The uncertainty of this estimate is considerable, however, and the lower bound of the 90% confidence interval is $\tau = 9{,}000$ yr.

This large return period should not be overstated, and is here merely used to express the rareness of such an extreme summer with respect to the long-term instrumental series available. In particular, the analysis does not exclude the possibility that such warm summers might have occurred in the more distant historical past,

for instance in the Medieval Warm Period[11], in 1540[12,13] or in 1757. It suggests, however, that an event like summer 2003 does not fit into the gaussian statistics spanned by the observations of the reference period, but might rather be associated with a transient change of the statistical distribution. This interpretation is consistent with the idea that small changes of the statistical distribution can yield pronounced changes in the incidence of extremes[7,14].

As a shift of the statistical distribution by the observed mean warming is unable to explain the record-breaking summer 2003, we hypothesize that the heatwave might be due to a change of the distribution's width, representing an increase in year-to-year variability. Support for this hypothesis comes from a regional climate model (RCM) driven by a greenhouse-gas scenario representing 2071–2100 conditions (SCEN). The scenario integration is compared against a control integration covering the period 1961–90 (CTRL). At the lateral boundaries, the RCM is driven by a model chain consisting of two general circulation models (GCMs; see Methods section for details). The use of a high-resolution RCM increases our ability to compare the results against observations.

The statistical temperature distribution for CTRL agrees notably well with observations. For the grid point in northern Switzerland, the summer climate is characterized by a temperature mean of $\bar{T} = 16.1\,^{\circ}\mathrm{C}$ and a standard deviation of $\sigma = 0.96\,^{\circ}\mathrm{C}$, while the long-term characteristics of our temperature series are $\bar{T} = 16.9\,^{\circ}\mathrm{C}$ and $\sigma = 0.94\,^{\circ}\mathrm{C}$.

Figure 3a, b displays JJA temperatures for the two integrations for a grid point in northern Switzerland. In the SCEN simulation, the distribution is shifted by ~4.6 °C towards warmer temperatures. More important, SCEN also exhibits a pronounced widening of its statistical distribution, with the standard deviation increasing by 102%. This widening is statistically highly significant ($P < 1\%$) and only slightly affected by the transient warming within the two periods (a revised estimate using detrended temperature series yields a somewhat smaller variability increase of 86%). The spatial distribution of the relative increase in variability (Fig. 3d) shows a pronounced signal throughout central and eastern Europe that is not directly linked to the simulated mean temperature change (Fig. 3c). More detailed analysis suggests that the warm summers of SCEN show signs of drought[15], with the semi-arid Mediterranean climate progressing towards central Europe. In SCEN, central Europe is more often (but not always) affected by summer droughts than in CTRL, and this implies an increase in variability. The drought conditions develop in response to large-scale anticyclonic forcing, and they nonlinearly amplify local temperature anomalies. During droughts the net balance of solar and infrared radiation is almost entirely balanced by local heating, while evapotranspiration

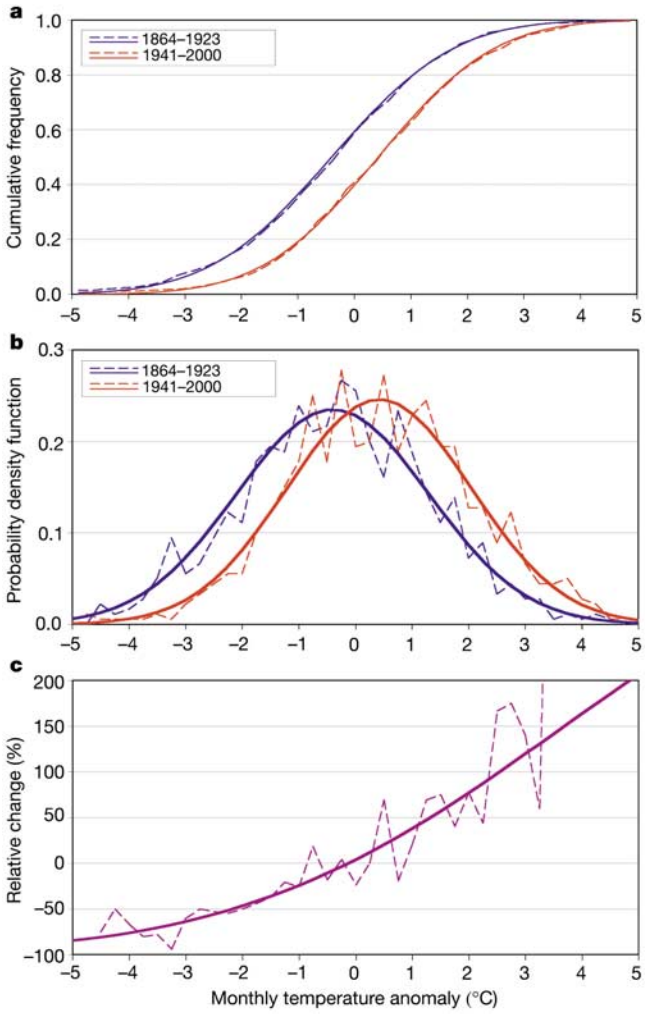

Figure 2 Statistical distribution of Swiss monthly temperature anomalies (compound statistics using January–December monthly data). Data in **a** and **b** are shown for the periods 1864–1923 (blue curves) and 1941–2000 (red curves). Panels show the cumulative frequency distribution (**a**), the probability density function (**b**), and the relative frequency change between the two periods (**c**). Full lines show the fit with the gaussian distribution, dashed lines are obtained from raw data.

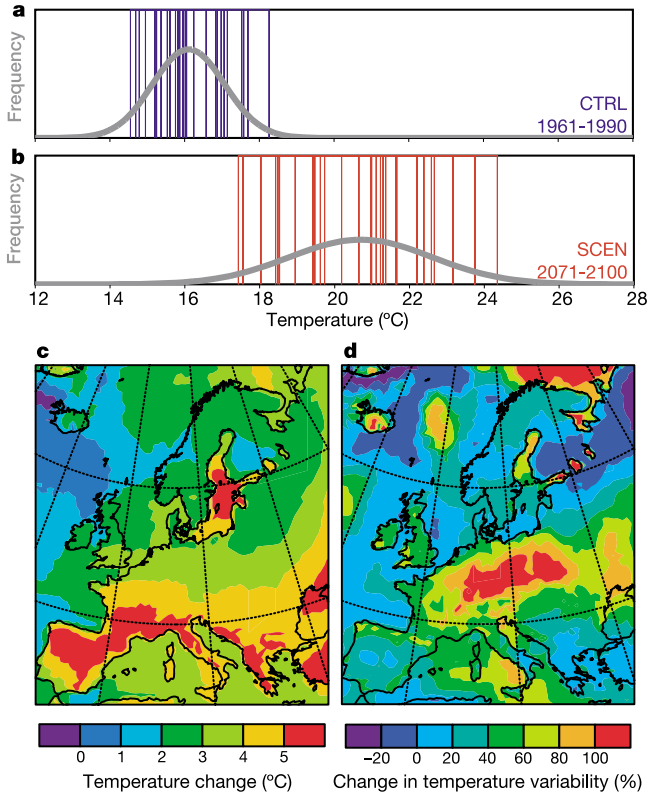

Figure 3 Results from an RCM climate change scenario representing current (CTRL 1961–90) and future (SCEN 2071–2100) conditions. **a**, **b**, Statistical distribution of summer temperatures at a grid point in northern Switzerland for CTRL and SCEN, respectively. **c**, Associated temperature change (SCEN–CTRL, °C). **d**, Change in variability expressed as relative change in standard deviation of JJA means ((SCEN–CTRL)/CTRL, %).

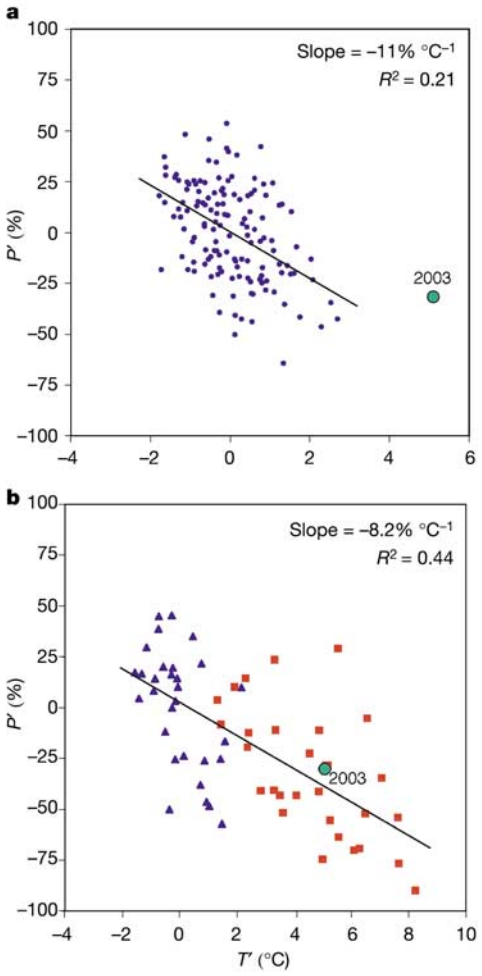

Figure 4 Scatter diagrams showing summer mean temperature and precipitation anomalies for northern Switzerland. **a**, Long-term (1864–2003) station data with respect to 1961–90 means. **b**, Climate change simulations CTRL (1961–90, blue symbols) and SCEN (2071–90, red symbols) with respect to CTRL means. The green symbols show the observations for JJA 2003. The regression lines in **a** and **b** are based on 1864–2002 data and combined CTRL and SCEN data, respectively.

is suppressed owing to the lack of soil moisture[16]. This process may be further amplified by a positive feedback between soil moisture and precipitation[17,18].

The sequence of feedbacks involves substantial uncertainties due to large-scale anticyclonic forcing[19], radiation[20], soil hydrology[21] and other processes, which are difficult to represent in climate models. To check on our simulations, we have analysed other GCM and RCM scenarios of greenhouse-gas conditions, and find that all of these exhibit a substantially increased level of variability over large parts of Europe (we have studied one GCM and four RCM simulations from the PRUDENCE project; http://prudence.dmi.dk).

The simulated increase in variability also implies an increase in extremes relative to mean climatic conditions. For illustration, a 50% increase in the standard deviation of our long-term JJA temperature series ($\sigma = 0.94\,^{\circ}\mathrm{C}$) would raise the probability of a 2003-like event ($T' = 3.85\,^{\circ}\mathrm{C}$ with respect to 1990–2002) by a factor of ~150. For an event with $T' = 5\,^{\circ}\mathrm{C}$, it would increase by a factor of ~5,100. This tremendous sensitivity of extremes to the width of the statistical distribution has led to the statement "variability is more important than averages"[14]. A recent increase in variability is thus a plausible hypothesis to explain extreme JJA 2003 conditions. Such a hypothesis would also be compatible with the occurrence of drastically different European summers such as in 2002 and 2003, but at present there are insufficient data to draw any firm conclusions.

To conclude, we address the question of whether the abnormal summer 2003 shows similar characteristics to those simulated in the RCM runs. To this end, summer temperature and precipitation anomalies are displayed against each other, both for the observations (Fig. 4a) and for the climate change simulations (Fig. 4b). Both panels include a data point representing observed JJA 2003 conditions, and the results apply to northern Switzerland. The observed data (Fig. 4a) are based on averages of conventional temperature and precipitation (rain-gauge) observations at the four stations referred to above, while the simulated data (Fig. 4b) are shown for a single grid point roughly corresponding to the location of our long-term series.

Several inferences can be drawn from the analysis. First, both data sets exhibit a similar (statistically significant) relationship between temperature and precipitation anomalies. The regression analysis yields slopes of $-11\%\,^{\circ}\mathrm{C}^{-1}$ and $-8.2\%\,^{\circ}\mathrm{C}^{-1}$ for the observations and the simulations, respectively. Thus, although there is some underestimation of summer precipitation in CTRL (at the grid point under consideration, by 21%), the simulations credibly represent the observed precipitation sensitivity. Despite a general trend towards drier conditions with increasing temperatures, there is also an increase in the incidence of heavy precipitation events[22].

Second, Fig. 4b demonstrates that in terms of temperature and precipitation the climatic conditions in JJA 2003 were not unlike those simulated by SCEN for the period 2071–2100. For northern Switzerland, the 2003 observation is located approximately in the middle of the SCEN data points (Fig. 4b). Thus, the RCM simulations suggest that towards the end of the century—under the given scenario assumptions—about every second summer could be as warm or warmer (and as dry or dryer) than 2003.

Our results demonstrate that the European summer climate might experience a pronounced increase in year-to-year variability in response to greenhouse-gas forcing. Such an increase in variability might be able to explain the unusual European summer 2003, and would strongly affect the incidence of heatwaves and droughts in the future. It would represent a serious challenge to adaptive response strategies designed to cope with climate change. □

Methods

Large-scale analysis of summer 2003

The continental-scale temperature anomaly for JJA 2003 (Fig. 1a) is based on ERA-40 reanalysis data[23] (for 1961–90) and operational meteorological analysis data (for 2003) of the European Centre for Medium-Range Weather Forecasts (ECMWF; see http://www.ecmwf.int). Monthly temperatures are computed as means of daily T_{min} and T_{max}. Small height differences between the ERA-40 and ECMWF topographies are accounted for by the use of an adiabatic lapse rate (0.6 °C per 100 m).

Estimation of return period

The stochastic concept adopted in the estimation of return periods assumes independent, identically distributed JJA temperatures with the underlying distribution being gaussian. The distribution parameters are estimated from the data of the reference period, using the method of moments (which in the case of a gaussian distribution is identical to maximum-likelihood estimation). The return period of the event (expected frequency of threshold exceedance) is then calculated from the fitted distribution. Confidence bounds of the return period were calculated by parametric resampling. These take into account the uncertainty of the parameter estimates given the finite sample size (that is, the number of summers in the reference period), but not the uncertainty in the underlying stochastic concept. We have also tested whether the data are reasonably gaussian distributed, checking quantile-quantile plots (see also Fig. 2a).

Climate change simulations

The climate change scenario is based on the SRES A2 transient greenhouse-gas scenario as specified by the Intergovernmental Panel on Climate Change (IPCC)[24]. The scenario computations involve three numerical models: the low-resolution HadCM3 global coupled atmosphere–ocean GCM, the intermediate-resolution HadAM3H atmospheric GCM, and the CHRM limited-area high-resolution RCM. The HadCM3 simulation[25,26] is a long integration using the observed atmospheric composition for 1859–1990 and scenario conditions for 1991–2100. For the HadAM3H simulation[27], two time-slice

experiments are available, representing control (1961–90) and scenario (2071–2100) conditions. The former is driven by observed sea surface temperature and sea-ice distributions, while the latter uses the changes from the HadCM3[28]. The CHRM RCM[29] is used with a horizontal resolution of 56 km and 20 levels in the vertical, and is driven at its lateral boundaries by HadAM3H. The CHRM has been validated regarding its ability to represent observed natural interannual variations[29]. The simulated increase in temperature variability in SCEN is largely determined by the soil hydrology of the model under consideration. For instance, it is substantially smaller in the CHRM than in the driving HadAM3H simulation.

Received 15 September; accepted 17 December 2003; doi:10.1038/nature02300.
Published online 11 January 2004.

1. Jones, P. D. & Moberg, A. Hemispheric and large-scale surface air temperature variations: An extensive revision and an update to 2001. *J. Clim.* **16,** 206–223 (2003).
2. Folland, C. K. *et al.* Global temperature change and its uncertainties since 1861. *Geophys. Res. Lett.* **28,** 2621–2624 (2001).
3. Crowley, T. J. Causes of climate change over the past 1000 years. *Science* **289,** 270–277 (2000).
4. Jones, P. D., Osborn, T. J. & Briffa, K. R. The evolution of climate over the last millennium. *Science* **292,** 662–667 (2001).
5. Easterling, D. R. *et al.* Observed variability and trends in extreme climate events: A brief review. *Bull. Am. Meteorol. Soc.* **81,** 417–425 (2000).
6. Frich, P. *et al.* Observed coherent changes in climatic extremes during the second half of the twentieth century. *Clim. Res.* **19,** 193–212 (2002).
7. Folland, C. K. *et al.* in *Climate Change 2001: The Scientific Basis* (eds Houghton, J. T. *et al.*) 99–182 (Cambridge Univ. Press, Cambridge, UK, 2001).
8. Aschwanden, A. *et al. Bereinigte Zeitreihen: Die Ergebnisse des Projekts KLIMA90* (MeteoSwiss, Zürich, 1996).
9. Bergert, M. *et al. Homogenisierung von Klimamessreihen und Berechnung der Normwerte 1961–1990* Veröffentlichungen der MeteoSchweiz, 67, MeteoSwiss, Zürich, (2003).
10. Allen, M. R. Liability for climate change. *Nature* **42,** 891–892 (2003).
11. Esper, J., Cook, E. R. & Schweingruber, F. H. Low-frequency signals in long tree-ring chronologies for reconstructing past temperature variability. *Science* **295,** 2250–2253 (2002).
12. Pfister, C. *et al.* Documentary evidence on climate in sixteenth-century Europe. *Clim. Change* **43,** 55–110 (1999).
13. Jacobeit, J., Wanner, H., Koslowski, G. & Gudd, M. European surface pressure patterns for months with outstanding climatic anomalies during the sixteenth century. *Clim. Change* **43,** 201–221 (1999).
14. Katz, R. W. & Brown, B. G. Extreme events in a changing climate: Variability is more important than averages. *Clim. Change* **21,** 289–302 (1992).
15. Wetherald, R. T. & Manabe, S. The mechanisms of summer dryness induced by greenhouse warming. *J. Clim.* **8,** 3096–3108 (1995).
16. Hartmann, D. L. *Global Physical Climatology* (Academic, San Diego, 1994).
17. Enthekabi, D., Rodriguez-Iturbe, I. & Bras, R. L. Variability in large-scale water balance with land surface-atmosphere interaction. *J. Clim.* **5,** 798–813 (1992).
18. Schär, C., Lüthi, D., Beyerle, U. & Heise, E. The soil-precipitation feedback: A process study with a regional climate model. *J. Clim.* **12,** 722–741 (1999).
19. Rodwell, M. J. & Hoskins, B. J. Subtropical anticyclones and summer monsoons. *J. Clim.* **14,** 3192–3211 (2001).
20. Wild, M., Dümenil, L. & Schulz, J. P. Regional climate simulation with a high resolution GCM: surface hydrology. *Clim. Dyn.* **12,** 755–774 (1996).
21. Seneviratne, S. I., Pal, J. S., Eltahir, E. A. B. & Schär, C. Summer dryness in the US midwest: A process study with a regional climate model. *Clim. Dyn.* **20,** 69–85 (2002).
22. Christensen, J. H. & Christensen, O. B. Severe summertime flooding in Europe. *Nature* **421,** 805–806 (2002).
23. Simmons, A. J. & Gibson, J. K. *The ERA-40 Project Plan* ERA-40 (Project Report Series, No. 1, ECMWF, Reading, 2000).
24. Nakicenovic, N. *et al. IPCC Special Report on Emissions Scenarios* (Cambridge Univ. Press, Cambridge, UK, 2000).
25. Johns, T. C. *et al.* Anthropogenic climate change for 1860 to 2100 simulated with the HadCM3 model under updated emissions scenarios. *Clim. Dyn.* **20,** 583–612 (2003).
26. Collins, M., Tett, S. F. B. & Cooper, C. The internal climate variability of HadCM3, a version of the Hadley Centre coupled model without flux adjustments. *Clim. Dyn.* **17,** 61–81 (2001).
27. Pope, D. V., Gallani, M., Rowntree, R. & Stratton, A. The impact of new physical parameterizations in the Hadley Centre climate model HadAM3. *Clim. Dyn.* **16,** 123–146 (2000).
28. Jones, R. G., Murphy, J. M., Hassell, D. C. & Taylor, R. *Ensemble Mean Changes in a Simulation of the European Climate of 2071–2100 Using the New Hadley Centre Regional Modelling system HadAM3H/HadRM3H* (Hadley Centre Report, Hadley Centre, Exeter, UK, 2001); available at ⟨http://prudence.dmi.dk⟩ (2001).
29. Vidale, P. L., Lüthi, D., Frei, C., Seneviratne, S. & Schär, C. Predictability and uncertainty in a regional climate model. *J. Geophys. Res. D* **108** doi:101029/2002JD002810 (2003).

Acknowledgements We thank the climatology and data teams of MeteoSwiss (Zürich, Switzerland) for providing access to their long-term homogenized temperature series, the Hadley Centre (Exeter, UK) for providing access to their climate change simulations, and the PRUDENCE team for access to climate simulations. We also thank our colleagues for comments on the manuscript. The computations were performed on the computing facilities of ETH and the Swiss Center for Scientific Computing (CSCS). This research was supported by the Fifth Framework Programme of the European Union (project PRUDENCE), by the Swiss Ministry for Education and Research, and by the Swiss National Science Foundation (NCCR Climate).

Competing interests statement The authors declare that they have no competing financial interests.

Correspondence and requests for materials should be addressed to C.S. (schaer@env.ethz.ch).

Reburial of fossil organic carbon in marine sediments

Angela F. Dickens[1,2], Yves Gélinas[3], Caroline A. Masiello[4,5], Stuart Wakeham[6] & John I. Hedges[1]

[1]*School of Oceanography, University of Washington, Box 355351, Seattle, Washington 98195-5351, USA*
[2]*Department of Chemistry, University of Washington, Box 351700, Seattle, Washington 98195-1700, USA*
[3]*Chemistry and Biochemistry Department, Concordia University, 1455 de Maisonneuve Boulevard West, Montreal (Quebec), Canada H3G 1M8*
[4]*Division of Geology and Planetary Sciences, Mail Code 170-25, California Institute of Technology, 1200 East California Boulevard, Pasadena, California 91125, USA*
[5]*Department of Geography, University of California Santa Barbara, Santa Barbara, California 93106, USA*
[6]*Skidaway Institute of Oceanography, 10 Ocean Science Circle, Savannah, Georgia 31411, USA*

Marine sediments act as the ultimate sink for organic carbon, sequestering otherwise rapidly cycling carbon for geologic timescales[1,2]. Sedimentary organic carbon burial appears to be controlled by oxygen exposure time *in situ*[3,4], and much research has focused on understanding the mechanisms of preservation of organic carbon[5]. In this context, combustion-derived black carbon has received attention as a form of refractory organic carbon that may be preferentially preserved in soils[6,7] and sediments[8,9]. However, little is understood about the environmental roles, transport and distribution of black carbon. Here we apply isotopic analyses to graphitic black carbon samples isolated from pre-industrial marine and terrestrial sediments. We find that this material is terrestrially derived and almost entirely depleted of radiocarbon, suggesting that it is graphite weathered from rocks, rather than a combustion product. The widespread presence of fossil graphitic black carbon in sediments has therefore probably led to significant overestimates of burial of combustion-derived black carbon in marine sediments. It could be responsible for biasing radiocarbon dating of sedimentary organic carbon, and also reveals a closed loop in the carbon cycle. Depending on its susceptibility to oxidation, this recycled carbon may be locked away from the biologically mediated carbon cycle for many geologic cycles.

Black carbon (BC) is the heterogeneous, aromatic and carbon-rich residue of biomass burning and fossil-fuel combustion[10,11]. It is formed on land, and may be eroded from soils and carried by rivers or via aerosol transport to the ocean. BC in open-ocean sediments is from 2,400 to 13,900 yr older than the co-deposited bulk organic carbon (OC)[12]. It is possible that BC is small and light enough to be stored in the oceanic dissolved organic carbon pool before being deposited in marine sediments, accounting for the older age of the BC. Alternatively, BC may age on land before transport to the ocean, either in the soil carbon pool or as fossil BC from ancient forest fires stored in rocks. Existing data cannot distinguish between these storage and transport mechanisms.

We examined marine sediments collected along a well-characterized transect perpendicular to the Washington coast[4], ranging from terrestrially influenced nearshore sites to marine-dominated offshore sediments. We determined sedimentary mixed layer depth using ^{210}Pb and sampled horizons (9–23 cm) deep enough beneath this layer to be pre-industrial according to ^{14}C sedimentation rates. The low levels of nuclides from nuclear fallout[13] and background levels of combustion-derived polycyclic aromatic hydrocarbons[14] present at our sampling depths in similar Washington slope samples further suggest that deeply mixed anthropogenic graphitic black carbon (GBC) is minimal in our samples. We extracted GBC, an